JACS
JOURNAL OF THE AMERICAN CHEMICAL SOCIETY

Communication

Exact stoichiometry of CeZr cornerstones in mixed-metal UiO-66 MOFs revealed by EXAFS spectroscopy

Kirill A. Lomachenko, Jannick Jacobsen, Aram L. Bugaev, Cesare Atzori, Francesca Bonino, Silvia Bordiga, Norbert Stock, and Carlo Lamberti

J. Am. Chem. Soc., **Just Accepted Manuscript** • DOI: 10.1021/jacs.8b10343 • Publication Date (Web): 30 Nov 2018

Just Accepted

ACS Publications

is published by the American Chemical Society. 1155 Sixteenth Street N.W., Washington, DC 20036

Exact stoichiometry of Ce_xZr_{6-x} cornerstones in mixed-metal UiO-66 MOFs revealed by EXAFS spectroscopy

Kirill A. Lomachenko,*[,1] Jannick Jacobsen,[2] Aram L. Bugaev,[3] Cesare Atzori,[4] Francesca Bonino,[4] Silvia Bordiga,[4] Norbert Stock[2] and Carlo Lamberti*[,3,5]

[1]European Synchrotron Radiation Facility, 71 Avenue des Martyrs, CS 40220, 38043 Grenoble Cedex 9, France

[2]Institut für Anorganische Chemie, Christian-Albrechts-Universität, Max-Eyth-Straße 2, D 24118 Kiel, Germany

[3]Smart Materials Research Institute, Southern Federal University, Sladkova 178/24, 344090 Rostov-on-Don, Russia

[4]Department of Chemistry, NIS interdepartmental Center and INSTM Reference Center, University of Turin, Via Quarello 15, 10135 Turin, Italy

[5]Department of Physics, INSTM Reference Center and CrisDi Interdepartmental Centre for Crystallography, University of Turin, Via P. Giuria 1, 10125 Turin Italy

Supporting Information Placeholder

ABSTRACT: Bimetallic Ce/Zr-UiO-66 MOFs proved to be promising materials for various catalytic redox applications, representing, together with other bimetallic MOFs, a new generation of porous structures. However, no direct proof for the presence of both metals in a single cornerstone of UiO-type MOFs was reported so far. Employing element-selective XAS techniques herein we demonstrate for the first time that our synthesis route allows obtaining Ce/Zr-UiO-66 MOFs with desired Ce content and bimetallic $CeZr_5$ cornerstones. Performing multiple-edge EXAFS analysis we determine the exact stoichiometry of the cornerstones, which explains the dependence of thermal and chemical stability of the materials on Ce content.

Among the numerous families of metal-organic frameworks (MOFs),[1-2] zirconium-based UiO-66, built of hexanuclear $[Zr_6(\mu_3\text{-}O)_4(\mu_3\text{-}OH)_4]^{12+}$ clusters connected by 1,4-benzene-dicarboxylate (BDC) linkers (Figure 1a) is known for its exceptional stability.[3-5] However, Zr clusters (Figure 1b) are chemically inactive due to the limited redox capabilities of zirconium. In contrast, cerium is known for applications in catalysis.[6] Recently synthesized Ce-UiO-66 and Ce-UiO-67 MOFs have already been successfully studied in various catalytical applications, exploiting Ce redox properties.[7-11] At the same time, temperature stability of Ce-UiO-66 MOFs is inferior compared to the original Zr-UiO-66 material. However, it increases for bimetallic Ce/Zr-UiO-66 MOFs containing low amounts of Ce(IV) ions, reaching up to 350 °C for the $Ce_{0.5}Zr_{5.5}$UiO-66 compound[12] and thus opening new perspectives for catalysis.[13-14]

Although metal substitution in different MOFs is widely discussed in the literature,[15-25] to the best of our knowledge, no direct proof for the existence of mixed-metal cornerstones in UiO-family MOFs have been presented so far. The cornerstones in mixed-metal compounds were only assumed to be either pure[26] or truly bimetallic[13] (Figure 1c,d). However, these chemically different cases were never discriminated.

The key to the quantitative determination of the cornerstone composition is the use of element-selective techniques, since the fine non-periodic variations of local atomic structure can hardly be detected by non-selective scattering-based methods. In this study, we provide the first direct proof of the existence of mixed-metal Ce/Zr cornerstones in Ce_xZr_{6-x}-UiO-66 MOFs, possible due to the combined analysis of Zr and Ce K-edge EXAFS data for the series of samples with different Ce content.

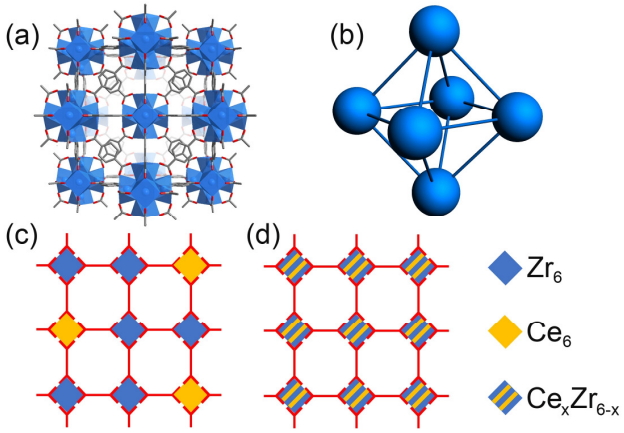

Figure 1 (a) Fragment of UiO-66 MOF structure; (b) Closeup on UiO-66 cornerstone (M atoms only); (c-d) representation of mixed-metal Ce_xZr_{6-x}-UiO-66 structure with pure (c) and bimetallic cornerstones (d).

The synthesis of the pure and mixed-metal Ce/Zr-UiO-66 compounds was performed following the previously reported procedures (SI, Section 1).[3,7,12] Ce content in the MOFs was determined by energy-dispersive X-ray spectroscopy (SI, Section 2 and Table S2). The mixed-metal samples will be referred to as CeXX in the discussion of the EXAFS results, XX being the fraction of Ce in the total metal content (in mol. %) determined by EDX.

Synchrotron PXRD measurements for desolvated pure Zr-, pure Ce- and bimetallic $Zr_{3.54}Ce_{2.46}$-UiO-66 MOFs were performed at ID22 beamline of the European Synchrotron Radiation Facility (ESRF) to determine with high precision their structural parameters, further used as the initial guess for the EXAFS refinement.

As a general tendency, the PXRD peak width decreases upon incorporation of Ce into the structure, thus the narrowest peaks were observed in the patterns of Ce-UiO-66 while Zr-UiO-66 exhibited the broadest ones, indicating the progressive increase of crystallite size with the rise of Ce content. The patterns indicate no symmetry-forbidden additional peaks due to nano-regions containing correlated lattice defects with reo topology[27] and are in perfect agreement with the *Fm*-3*m* space group (Figures S1-3 and Table S3). Hence, both Ce and Zr atoms, as well as the cluster and/or linker vacancies for all the investigated samples are randomly distributed throughout the crystal. The occurrence of large domains with lower crystalline symmetry, as well as the formation of crystalline extra-phases, is thus ruled out. Concomitantly, TGA and BET measurements previously reported for analogous Ce/Zr-UiO-66 MOFs evidenced that substitution of Zr with Ce is not accompanied by a significant rise of missing linker defects, resulting in maximum one missing linker per cornerstone.[12] Thus, it is not the defects, but the local composition of the clusters that has the major influence on the EXAFS data discussed below.

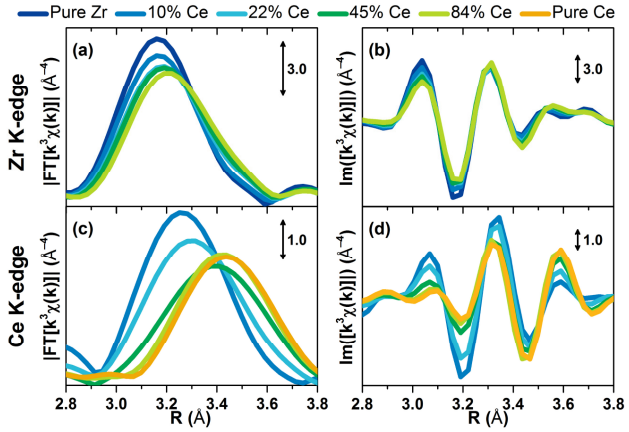

Figure 2 Closeup on the second shell peak in the modulus (a,c) and imaginary part (b,d) of not-phase-corrected Fourier transforms of k^3-weighted EXAFS data collected at Zr (a,b) and Ce K-edges (c,d) for the pure and mixed-metal UiO-66 MOFs.

Ce and Zr K-edge EXAFS as well as Ce L_3 XANES spectra were collected at BM31[28] and BM23[29] beamlines of ESRF, measuring as-prepared compounds at room temperature. Ce L_3-edge XANES data for all Ce-containing samples show the pure Ce(IV) phase (indicatively more than 95% of Ce content), confirming the success of the synthesis (Figure S4a). Differences between the XANES spectra of all MOFs at the three edges were minor, indicating that the electronic structure of neither Ce nor Zr species was significantly altered at different Ce:Zr ratios and excluding the possibility to draw structural conclusions from the in-depth XANES analysis (Figure S4).

Fourier-transformed Zr and Ce K-edge EXAFS data for all MOFs are shown in the Figure S6. The spectra are in agreement with those reported previously for Zr-UiO-66 MOFs[4,30] and for Ce clusters with the geometry similar to the UiO-type cornerstones.[31] The shape of the peaks in 1.2-2.5 Å range, originating mainly from M-O scattering (M being Zr or Ce), does not change significantly upon the increase of Ce content, which evidences rather small variations in O-coordination of Zr and Ce atoms. However, very pronounced changes are observed in the position and intensity of the second peak (2.8-3.8 Å), which appears due to the M-M scattering from the members of M_6 cornerstones (Figure 1b). It clearly indicates that the average values of M-M interatomic distances and the corresponding disorder depend on Ce:Zr ratio, which confirms the formation of mixed-metal Ce_xZr_{6-x} cornerstones.

Figure 2a,c presents a closeup on the second EXAFS peak of all the studied MOFs. Changes that take place upon introduction of Ce may be explained by assuming the preferential formation of $CeZr_5$ clusters, accompanied by pure Zr_6 or Ce_6 cornerstones in the proportion dictated by the total stoichiometry of the sample. This implies a coexistence of $CeZr_5$ and Zr_6 clusters for Ce contents lower than 17% (i.e. 1/6) and a mixture of $CeZr_5$ and Ce_6 for higher Ce loadings.

For the pure Zr MOF, the Zr-Zr distances in the cornerstones are highly homogeneous, leading to the maximum intensity of the Zr-Zr peak in the absence of static disorder. Upon the introduction of Ce, the formation of $CeZr_5$ clusters would cause progressive loss of intensity at Zr K-edge compared to the pure Zr MOF due to the splitting of the Zr-Zr coordination shell into Zr-Ce and Zr-Zr subshells with significantly different Zr-M distances, in agreement to the data for Ce10 and Ce22 samples (Figure 2a). The minimum should be reached at Ce content around 17%, where all cornerstones are represented by the $CeZr_5$ clusters. At the same time, at the Ce K-edge the intensity of the Ce-M peak would be at its maximum for low-Ce samples, since static and dynamic disorder of the Ce-Zr distances in the $CeZr_5$ clusters is expected to be quite low and comparable to the one of Zr-Zr in pure Zr clusters, while the Ce-Zr distance is likely to be shorter than the Ce-Ce one. For Ce loadings higher than 17%, the data evidence against the formation of mixed clusters with more than one Ce atom, but rather suggest that mainly pure Ce_6 cornerstones are formed from the excess of Ce, in addition to the $CeZr_5$ clusters. Indeed, that would explain the lack of major changes at the Zr K-edge between Ce22, Ce45 and Ce84 samples, since in such case all the Zr atoms in the material would be present as a part of $CeZr_5$ cornerstones and it is only the abundance of such cornerstones that would change with the increase of Ce content, but not their composition. Concomitantly, pure Ce_6 clusters are expected to have longer and less homogenous Ce-Ce distances compared to Ce-Zr and Zr-Zr ones in Zr_6 and $CeZr_5$ clusters, resulting in a shift of the second EXAFS peak at Ce K-edge to higher R and a decrease of its intensity.

Imaginary parts of the Ce K-edge EXAFS Fourier transforms (Figure 2d) indicate that it is the relative abundance of contributing Ce-Zr and Ce-Ce paths that changes at different Ce content rather than the lengths of these paths. Indeed, no significant shift of the oscillations is observed upon the increase of Ce content, but rather the redistribution of intensity from R = 3.1 Å region, where contribution of Ce-Zr scattering should be dominant, to R = 3.6 Å, where Ce-Ce signal is the strongest (given distances are not phase-corrected).

Hypothesis about the preferential formation of $CeZr_5$ cornerstones, put forward after the qualitative analysis of the EXAFS data was confirmed by quantitative EXAFS fitting at Zr and Ce K-edges. All ten EXAFS datasets (five at each edge) were fitted together, leading to the calculation of a global R-factor. Degeneracies of M-M paths for bimetallic MOFs were calculated from the elemental composition data provided by EDX analysis assuming preferential formation of the $CeZr_5$ cornerstones (SI, Section 4.4). Results of the combined EXAFS fitting of ten independent datasets are shown in Figure 3, while the values of the obtained fitting parameters are reported in Table 1.

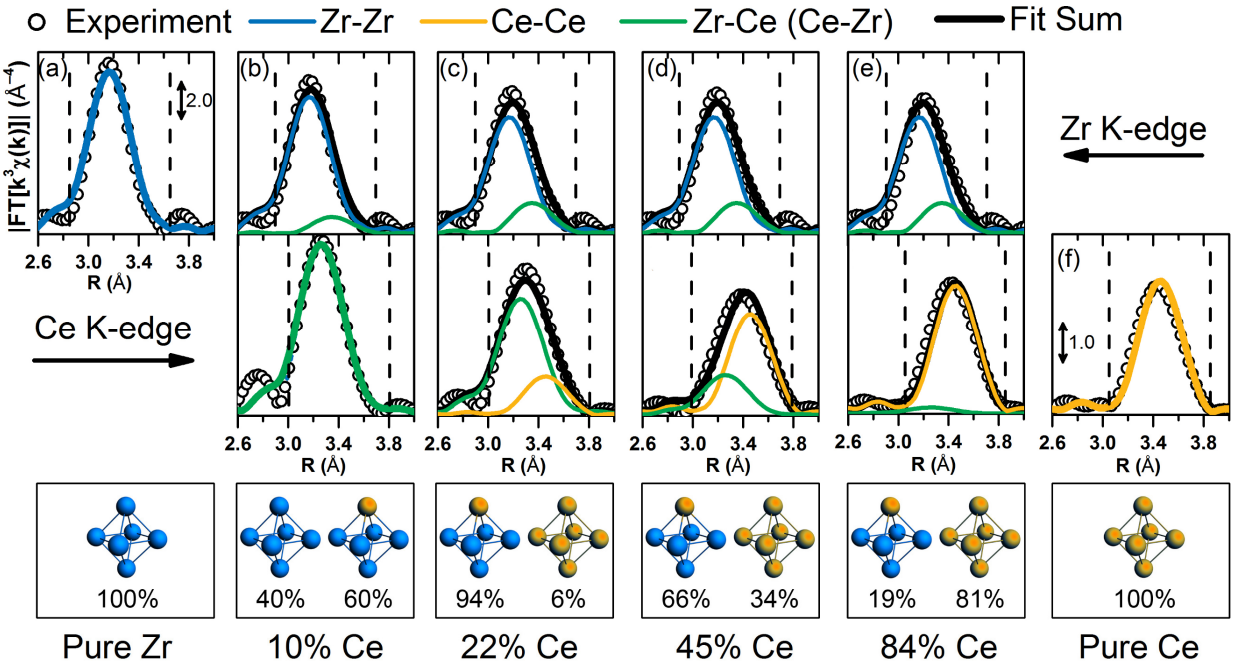

Figure 3 Results of the EXAFS fitting. Experimental data are shown as white circles, fitted curves are presented as full lines. Zr-Zr contribution – blue, Ce-Ce contribution – yellow, Zr-Ce and Ce-Zr contribution – green. For mixed-metal MOFs, the sum of the two contributions is shown in black. Bottom panels summarize the cornerstone composition employed for fitting the spectra of each sample.

Table 1 Best-fit parameters obtained by combined EXAFS fitting of ten datasets at both Zr and Ce K-edges. M-M interatomic distances obtained from PXRD refinement are shown in parentheses.

Parameter	Value
R-factor	0.012
N_{ind}	63.1
N_{par}	11
S_0^2	1.0 ± 0.1
ΔE_{Ce}, eV	0.9 ± 1.1
ΔE_{Zr}, eV	0.6 ± 0.7
$R_{Ce\text{-}Zr}$, Å	3.653 ± 0.004
$\sigma^2_{Ce\text{-}Zr}$, Å^2	0.0050 ± 0.0002
$R_{Ce\text{-}Ce}$, Å^2	3.784 ± 0.004 (3.78)
$\sigma^2_{Ce\text{-}Ce}$, Å^2	0.0060 ± 0.0002
$R_{Zr\text{-}Zr}$, Å	3.529 ± 0.003
$\sigma^2_{Zr\text{-}Zr}$, Å^2	0.0050 ± 0.0002
R_{Zr6}, Å	3.525 ± 0.003 (3.51)
σ^2_{Zr6}, Å^2	0.0046 ± 0.0002

The fit shows excellent overall agreement with the experiment (see SI Section 4.4 for details). Obtained DW factors demonstrate that the extent of structural disorder depends on the composition of the cluster. The lowest DW factor $\sigma^2_{Zr6} = 0.0046$ Å^2 was obtained for the Zr-Zr path in pure Zr_6 cornerstones, which were expected to be the most rigid and ordered ones. Inclusion of one Ce atom in the cornerstone increases very slightly the inhomogeneity of the Zr-Zr and Zr-Ce distances, justifying the small rise of the corresponding DW factors to $\sigma^2_{Zr\text{-}Zr} = \sigma^2_{Ce\text{-}Zr} = 0.0050$ Å^2. For the Ce-Ce path, the EXAFS fit results in DW factor $\sigma^2_{Ce\text{-}Ce} = 0.0060$ Å^2, which is roughly 20% higher compared to those for Zr-Zr and Zr-Ce pairs.

The preferential formation of $CeZr_5$ cornerstones explains the trends in the stability of bimetallic UiO-66 MOFs with different Ce content reported by Lammert et al.[12] Indeed, while at low Ce loadings stability was decreasing linearly with the increase of Ce content, at around 20% it stabilized at the value observed for pure Ce-UiO-66 MOF. According to the current EXAFS analysis, this coincides with the disappearance of pure Zr_6 cornerstones, which, due to lower disorder and higher stability compared to Ce_6 and $CeZr_5$ cornerstones, increase the decomposition temperature of the material.

The preferential formation of $CeZr_5$ cornerstones over other mixed-metal clusters is partially in line with the recent theoretical calculations, that show that as a general trend, the mixing energy of the bimetallic cluster increases with the number of bimetallic edges.[32] However, the mixing energy for all possible structures of Ce_xZr_{6-x} cornerstone was reported to be positive,[32] suggesting that the most favorable configuration of Ce/Zr-UiO-66 MOF would contain only Zr_6 and Ce_6 cornerstones. Our DFT calculations also evidence that energetically the most favorable way to accommodate Ce atoms in the structure would be the formation of Ce_6 cornerstones (SI Section 5). In such case, though, the Ce and Zr K-edge EXAFS spectra would not be changing with Ce content. Therefore, the formation of the MOF structure must have more complex drivers, requiring the inclusion of additional factors (temperature, pressure, solvent effects) into the computational model. The high level of complexity of this computational task highlights the value of experimental methods for the determination of the composition of bimetallic MOFs.

To summarize, combined Ce and Zr K-edge EXAFS analysis demonstrates that in bimetallic Ce/Zr-UiO-66 MOFs mixed-metal $CeZr_5$ cornerstones coexist with pure Zr_6 (at Ce content lower than ca. 17%) and Ce_6 ones (at higher Ce content). The relative abundance of pure and bimetallic cornerstones is in both cases determined primarily by sample stoichiometry. Such observation serves as the first direct proof for the existence of mixed ZrCe cornerstones in the Ce/Zr-UiO-66 MOFs and allows to explain the previously-reported non-trivial dependence of temperature stability of these MOFs on Ce content.

ASSOCIATED CONTENT

Supporting Information

The Supporting Information is available free of charge on the ACS Publications website.
Experimental and data analysis details (PDF)

AUTHOR INFORMATION

Corresponding Authors

*kirill.lomachenko@esrf.fr, carlo.lamberti@unito.it

Notes

The authors declare no competing financial interests.

ACKNOWLEDGMENT

The authors are grateful to M. Brunelli, H. Emerich, W. van Beek, V. Dmitriev, O. Mathon and A. Fitch for the support during the experiments at BM31, BM23 and ID22 beamlines of the ESRF. We would like to thank B. Bueken, S. Smolders and A. Venier for the help with the XAS measurements, and H. Reinsch and N. Heidenreich for the assistance with PXRD experiment and data analysis. ALB acknowledges financial support by Russian Science Foundation project 18-73-00189.

REFERENCES

(1) Yaghi, O. M.; O'Keeffe, M.; Ockwig, N. W.; Chae, H. K.; Eddaoudi, M.; Kim, J. Reticular synthesis and the design of new materials. *Nature* **2003**, *423*, 705.

(2) Butova, V. V.; Soldatov, M. A.; Guda, A. A.; Lomachenko, K. A.; Lamberti, C. Metal-Organic Frameworks: Structure, Properties, Synthesis, and Characterization. *Russ. Chem. Rev.* **2016**, *85*, 280.

(3) Cavka, J. H.; Jakobsen, S.; Olsbye, U.; Guillou, N.; Lamberti, C.; Bordiga, S.; Lillerud, K. P. A New Zirconium Inorganic Building Brick Forming Metal Organic Frameworks with Exceptional Stability. *J. Am. Chem. Soc.* **2008**, *130*, 13850.

(4) Valenzano, L.; Civalleri, B.; Chavan, S.; Bordiga, S.; Nilsen, M. H.; Jakobsen, S.; Lillerud, K. P.; Lamberti, C. Disclosing the Complex Structure of UiO-66 Metal Organic Framework: A Synergic Combination of Experiment and Theory. *Chem. Mater.* **2011**, *23*, 1700.

(5) Shearer, G. C.; Chavan, S.; Ethiraj, J.; Vitillo, J. G.; Svelle, S.; Olsbye, U.; Lamberti, C.; Bordiga, S.; Lillerud, K. P. Tuned to Perfection: Ironing Out the Defects in Metal–Organic Framework UiO-66. *Chem. Mater.* **2014**, *26*, 4068.

(6) Montini, T.; Melchionna, M.; Monai, M.; Fornasiero, P. Fundamentals and Catalytic Applications of CeO2-Based Materials. *Chem. Rev.* **2016**, *116*, 5987.

(7) Lammert, M.; Wharmby, M. T.; Smolders, S.; Bueken, B.; Lieb, A.; Lomachenko, K. A.; Vos, D. D.; Stock, N. Cerium-based metal organic frameworks with UiO-66 architecture: synthesis, properties and redox catalytic activity. *Chem. Commun.* **2015**, *51*, 12578.

(8) Dalapati, R.; Sakthivel, B.; Ghosalya, M. K.; Dhakshinamoorthy, A.; Biswas, S. A cerium-based metal–organic framework having inherent oxidase-like activity applicable for colorimetric sensing of biothiols and aerobic oxidation of thiols. *CrystEngComm* **2017**, *19*, 5915.

(9) Dalapati, R.; Sakthivel, B.; Dhakshinamoorthy, A.; Buragohain, A.; Bhunia, A.; Janiak, C.; Biswas, S. A highly stable dimethyl-functionalized Ce(IV)-based UiO-66 metal–organic framework material for gas sorption and redox catalysis. *CrystEngComm* **2016**, *18*, 7855.

(10) Buragohain, A.; Biswas, S. Cerium-based azide- and nitro-functionalized UiO-66 frameworks as turn-on fluorescent probes for the sensing of hydrogen sulphide. *CrystEngComm* **2016**, *18*, 4374.

(11) Smolders, S.; Lomachenko, K. A.; Bueken, B.; Struyf, A.; Bugaev, A. L.; Atzori, C.; Stock, N.; Lamberti, C.; Roeffaers, M. B. J.; De Vos, D. E. Unravelling the Redox-catalytic Behavior of Ce^{4+} Metal-Organic Frameworks by X-ray Absorption Spectroscopy. *ChemPhysChem* **2018**, *19*, 373.

(12) Lammert, M.; Glißmann, C.; Stock, N. Tuning the stability of bimetallic Ce(IV)/Zr(IV)-based MOFs with UiO-66 and MOF-808 structures. *Dalton Trans.* **2017**, *46*, 2425.

(13) Nouar, F.; Breeze, M. I.; Campo, B. C.; Vimont, A.; Clet, G.; Daturi, M.; Devic, T.; Walton, R. I.; Serre, C. Tuning the properties of the UiO-66 metal organic framework by Ce substitution. *Chem. Commun.* **2015**, *51*, 14458.

(14) Ebrahim, A. M.; Bandosz, T. J. Ce(III) Doped Zr-Based MOFs as Excellent NO_2 Adsorbents at Ambient Conditions. *ACS Appl. Mater. Interfaces* **2013**, *5*, 10565.

(15) Liu, Q.; Cong, H.; Deng, H. Deciphering the Spatial Arrangement of Metals and Correlation to Reactivity in Multivariate Metal–Organic Frameworks. *J. Am. Chem. Soc.* **2016**, *138*, 13822.

(16) Lee, Y.; Kim, S.; Kang, J. K.; Cohen, S. M. Photocatalytic CO_2 reduction by a mixed metal (Zr/Ti), mixed ligand metal–organic framework under visible light irradiation. *Chem. Commun.* **2015**, *51*, 5735.

(17) He, J.; Zhang, Y.; He, J.; Zeng, X.; Hou, X.; Long, Z. Enhancement of photoredox catalytic properties of porphyrinic metal–organic frameworks based on titanium incorporation via post-synthetic modification. *Chem. Commun.* **2018**, *54*, 8610.

(18) Tu, J.; Zeng, X.; Xu, F.; Wu, X.; Tian, Y.; Hou, X.; Long, Z. Microwave-induced fast incorporation of titanium into UiO-66 metal–organic frameworks for enhanced photocatalytic properties. *Chem. Commun.* **2017**, *53*, 3361.

(19) Szeto, K. C.; Lillerud, K. P.; Tilset, M.; Bjørgen, M.; Prestipino, C.; Zecchina, A.; Lamberti, C.; Bordiga, S. A Thermally Stable Pt/Y-Based Metal−Organic Framework: Exploring the Accessibility of the Metal Centers with Spectroscopic Methods Using H_2O, CH_3OH, and CH_3CN as Probes. *J. Phys. Chem. B* **2006**, *110*, 21509.

(20) Szeto, K. C.; Prestipino, C.; Lamberti, C.; Zecchina, A.; Bordiga, S.; Bjørgen, M.; Tilset, M.; Lillerud, K. P. Characterization of a New Porous Pt-Containing Metal-Organic Framework Containing Potentially Catalytically Active Sites: Local Electronic Structure at the Metal Centers. *Chem. Mater.* **2007**, *19*, 211.

(21) Brozek, C. K.; Dincă, M. Ti^{3+}-, $V^{2+/3+}$-, $Cr^{2+/3+}$-, Mn^{2+}-, and Fe^{2+}-Substituted MOF-5 and Redox Reactivity in Cr- and Fe-MOF-5. *J. Am. Chem. Soc.* **2013**, *135*, 12886.

(22) Brozek, C. K.; Dincă, M. Cation exchange at the secondary building units of metal–organic frameworks. *Chem. Soc. Rev.* **2014**, *43*, 5456.

(23) Vuong, G.-T.; Pham, M.-H.; Do, T.-O. Synthesis and engineering porosity of a mixed metal Fe_2Ni MIL-88B metal–organic framework. *Dalton Trans.* **2013**, *42*, 550.

(24) Stubbs, A. W.; Braglia, L.; Borfecchia, E.; Meyer, R. J.; Román-Leshkov, Y.; Lamberti, C.; Dincă, M. Selective Catalytic Olefin Epoxidation with Mn^{II}-Exchanged MOF-5. *ACS Catal.* **2018**, *8*, 596.

(25) Butova, V. V.; Polyakov, V. A.; Budnyk, A. P.; Aboraia, A. M.; Bulanova, E. A.; Guda, A. A.; Reshetnikova, E. A.; Podkovyrina, Y. S.; Lamberti, C.; Soldatov, A. V. Zn/Co ZIF family: MW synthesis, characterization and stability upon halogen sorption. *Polyhedron* **2018**, *154*, 457.

(26) Kim, M.; Cahill, J. F.; Fei, H.; Prather, K. A.; Cohen, S. M. Postsynthetic Ligand and Cation Exchange in Robust Metal–Organic Frameworks. *J. Am. Chem. Soc.* **2012**, *134*, 18082.

(27) Cliffe, M. J.; Wan, W.; Zou, X.; Chater, P. A.; Kleppe, A. K.; Tucker, M. G.; Wilhelm, H.; Funnell, N. P.; Coudert, F.-X.; Goodwin, A. L. Correlated defect nanoregions in a metal–organic framework. *Nat. Commun.* **2014**, *5*, 4176.

(28) Abdala, P. M.; Safonova, O. V.; Wiker, G.; van Beek, W.; Emerich, H.; van Bokhoven, J. A.; Sá, J.; Szlachetko, J.; Nachtegaal, M. Scientific Opportunities for Heterogeneous Catalysis Research at the SuperXAS and SNBL Beam Lines. *CHIMIA* **2012**, *66*, 699.

(29) Mathon, O.; Beteva, A.; Borrel, J.; Bugnazet, D.; Gatla, S.; Hino, R.; Kantor, I.; Mairs, T.; Munoz, M.; Pasternak, S.; Perrin, F.; Pascarelli, S. The time-resolved and extreme conditions XAS (TEXAS) facility at the European Synchrotron Radiation Facility: the general-purpose EXAFS bending-magnet beamline BM23. *J. Synchrotron Rad.* **2015**, *22*, 1548.

(30) Plonka, A. M.; Wang, Q.; Gordon, W. O.; Balboa, A.; Troya, D.; Guo, W.; Sharp, C. H.; Senanayake, S. D.; Morris, J. R.; Hill, C. L.; Frenkel, A. I. In Situ Probes of Capture and Decomposition of Chemical Warfare Agent Simulants by Zr-Based Metal Organic Frameworks. *J. Am. Chem. Soc.* **2017**, *139*, 599.

(31) Hennig, C.; Ikeda-Ohno, A.; Kraus, W.; Weiss, S.; Pattison, P.; Emerich, H.; Abdala, P. M.; Scheinost, A. C. Crystal Structure and Solution Species of Ce(III) and Ce(IV) Formates: From Mononuclear to Hexanuclear Complexes. *Inorg. Chem.* **2013**, *52*, 11734.

(32) Trousselet, F.; Archereau, A.; Boutin, A.; Coudert, F.-X. Heterometallic Metal–Organic Frameworks of MOF-5 and UiO-66 Families: Insight from Computational Chemistry. *J. Phys. Chem. C* **2016**, *120*, 24885.

Insert Table of Contents artwork here